Exploring the Mechanism of the Electrochemical Polymerization of CO_2 to hard carbon over CeO_2(110)

Florian Keller[†‡], Johannes Döhn[†], Axel Groß[†] , Michael Busch[†*]

Conversion of CO_2 to hard carbon is an interesting technology for the removal of carbon dioxide from the atmosphere. Recently, it was shown that CeO_2 can selectively catalyse this reaction but we still lack information regarding the reaction mechanism. Using density functional theory (DFT) modelling we explore possible reaction mechanisms that allow for the polymerization of CO_2. According to our computations the reaction is initialized by the adsorption of CO_2 in an oxygen vacancy. Owing to the rich defect chemistry of ceria a large number of suitable sites are available at the surface. C-C bond formation is achieved through an aldol condensation type mechanism which comprises the electrochemical elimination of water to form a carbene. This carbene then performs a nucleophilic attack on CO_2. The reaction mechanism possesses significant similarities to the corresponding reaction in synthetic organic chemistry. Since the mechanism is completely generic it allows for all relevant steps of the formation of hard carbon like chain growth, chain linkage and the formation of side chains or aromatic rings. Surprisingly, ceria mainly serves as an anchor for CO_2 in an oxygen vacancy while all other subsequent reaction steps are almost completely independent from the catalyst. These insights are important for the development of novel catalysts for CO_2 reduction and may also lead to new reactions for the electrosynthesis of organic molecules.

1 Introduction

With the increase in global greenhouse gas emissions[1,2] an increasing number of severe consequences of global warming have become apparent in recent years. To minimize their impact on the world's population, it is crucial to find methods to effectively capture, convert and store CO_2. A promising technology to achieve this are negative emission technologies (NETs).[3,4] NETs range from biological conversion of CO_2 into biomass through microorganisms,[5,6] algae[5,6] or afforestation[7,8] to air capture followed by direct CO_2 storage[7,9] or chemical[10,11] and electrochemical[5,6,8,12] conversion into long-term stable materials such as oxalates[13,14] or hard carbon[4] and carbon fibres.[15]

Unfortunately, chemical storage of CO_2 as oxalate requires high pressures, a sacrificial reducing agent and the introduction of a counter ion such as Ca^{2+}[16,17] which renders them technically demanding. Similarly also other chemical and electrochemical routes for CO_2 conversion into non-volatile products like the synthesis of hard carbon still face severe challenges. To complicate the situation even more, the methods currently considered for CO_2 reduction must be sustainable themselves[18] while at the same time scalable to convert several gigatons of CO_2 per year.[19] Accordingly, any meaningful process must rely on abundant materials and in itself be CO_2 neutral. Furthermore, to completely remove CO_2 from the atmosphere it is insufficient to convert it into hydrocarbons or alcohols since their combustion again results in CO_2.[20,21]

Indeed, most processes for CO_2 reduction typically target precisely these products.[20,21] An example of this is the chemical synthesis of methanol from CO_2 and H_2 using Cu/Zn/Al[22–24] or In oxide[25] catalysts. For electrochemical CO_2 reduction on the other hand a very diverse set of materials which includes both homogeneous[26–30] and heterogeneous[30–33] catalysts has been proposed. Typical examples of homogeneous catalysts are transition metals coordinated by porphyrin[34–41] or phthalocyanine.[42,43] However, these catalyst are again mostly selective for CO or post-CO products like methane or simple C_2 and C_3 compounds which are unsuitable for NETs. The same is also true for common heterogeneous catalysts like transition metal doped graphene[44,45] or metallic Cu.[46,47] Indeed, the formation of oxalates has only been reported for few materials like Hg[48] or Pb[49] but the validity of some of these results was questioned recently.[50]

On the other hand a catalyst which converts CO_2 electrochemically to hard carbon was, to the best of our knowledge, absent until the recent seminal work of Esrafilzadeh et al.[51].

[†] *Institute of Theoretical Chemistry, Ulm University, Oberberghof 7, 89081 Ulm, Germany; E-mail: michael.busch@uni-ulm.de*

[‡] *Current Adress: Institut für Chemie (IFC), University of Zurich, Winterthurerstrasse 190, 8057 Zürich, Switzerland*

† Electronic Supplementary Information (ESI) available: The SI includes a detailed summary of all considered mechanisms, a description of the computational methods, a rational for using GGA functionals for CeO_2 and the PDOS See DOI: 00.0000/00000000.

They found that liquid Galinstan (GaInSn alloy) in 2M H_2O/N,N-dimethylformamide (DMF) selectively catalyses the electrochemical reduction to hard carbon with a moderately high onset overpotential of -310 mV. However, the current remains far below 1 mA/cm^2 up to an overpotential of roughly -1.3 V.[51] Thus, it is fair to say that despite the very low reported onset potential almost no CO_2 reduction takes place until a much lower potential is reached. The authors hypothesized that a Ce oxide is the active material but no proof was provided.[51] In addition to the nature of the catalyst also the mechanism through which the reaction proceeds is so far unknown.

In what follows we will evaluate the reaction mechanism for the polymerization of CO_2 to carbonaceous materials over CeO_2(110) using density functional theory calculations. Our computations indicate, that CeO_2(110) possesses an oxygen defect rich surface under reaction conditions. We will show that these defects are indeed central for its reactivity. C-C bond formation proceeds through a simple electrochemical aldol condensation type mechanism. These results provide critical insights for the design of more efficient catalysts for the electrochemical reduction of CO_2 to hard carbon and may also inspire new reactions for electro-synthetic routes to organic compounds.

2 Computational Details

2.1 Surfaces

All DFT calculations were performed using the PBE[52] generalized gradient approximation (GGA) functional with Grimme D3 corrections[53–55] as implemented into the Vienna ab-initio simulation package (VASP Version 5.4.1).[56] To evaluate the validity of our results also PBE+U-D3 calculations with a Hubbard U[57,58] were performed for selected cases. Following previous work[59] a Hubbard U of 4.5 eV was used. However, if not stated explicitly otherwise, no semi-empirical Hubbard-U corrections were added. A detailed discussion on the benefits of using a GGA ansatz for these types of materials can be found in the SI.

The electronic wave functions were expanded in plane waves with energies up to 650 eV and the convergence threshold was set to 10^{-6} eV. Convergence of the electronic structure calculations was aided by adding a Gaussian smearing of 0.1 eV. Core electrons were approximated with projector augmented wavefunctions (PAW).[60] The structure was considered converged if the Hellman-Feynman forces were below 10^{-2} eV/Å. The bulk-structures were optimized using a 5x5x5 k-point set. 1x1 surfaces were calculated using a 6x6x1 k-point mesh, while the k-point sampling was reduced to 3x6x1 for the 2x1 slabs and to 3x3x1 for the 2x2-sized slabs. Conversion from electronic to Gibbs Free energies was achieved by addition of constant corrections for zero-point energies and entropies using the values reported by Chan et al.[61] and Nørskov et al.[62] The numeric values of each contribution are summarized in the supplementary information (See SI Table S1).

Attempts to include solvent effects through implicit solvents failed owing to well known instabilities in VASPsol[63–65] for cerium oxides.[66] We therefore attempted to obtain solvation energies by performing single point computations using the SCCS model[67] implemented into CP2K (version: 9.1).[68] However, we were unable to converge the wave function. Similarly also attempts to obtain solvation energies using CANDLE[69] and GLSSA13[69–71] implemented into jDFTx (version: 1.7.0)[72] failed owing to severe instabilities in the wave functions for the GLSSA13 model which resulted in unphysical solvation energy differences of up to -150 eV between different intermediates. For CANDLE on the other hand constantly similarly unphysical solvation energies of the order to 0.1 eV were obtained. Accordingly we resorted to reporting gas phase energies. This is a common simplification in computational electrochemistry which still yields reasonable reaction energies.[45,73–78]

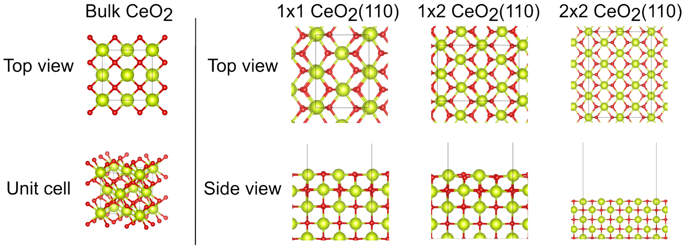

Fig. 1 Depiction of bulk and surface arrangements of CeO_2. Ce: lime, C: brown and O: red.

2.2 Acid Dissociation Constants

pK_a values of the carbonate species in DMF were computed using the isodesmic method[79–81] in combination with the recently introduced method to predict proton solvation energies in non-aqueous solvents.[81,82] For a detailed description of the methods and benchmarks we refer the reader to our previous work.[81,82] Identical to these studies, the dissociation of formic acid (pK_a in water: 3.77[83]) was used as reference reaction and the computed pK_a values (p$K_{a(comp)}$) were, following earlier work,[81] scaled to correct for shortcomings of the implicit solvation model using

$$pK_a = 0.75pK_{a\ (comp)} + 3.2 \qquad (1)$$

The DFT computations necessary for the determination of pK_a values were performed using Gaussian16 (Rev C.01)[84] with the M06-2X functional[85] and a 6-311++G∗∗ basis set with diffuse and polarization functions on all atoms. Structures were considered converged if no imaginary frequencies were present. Solvation effects were included through the implicit SMD[86] solvation model for water and DMF as implemented into Gaussian 16. Hydrogen was computed in the gas phase.

3 Results and Discussion

3.1 Active Species

It is commonly assumed that CO_2 reduction proceeds through the direct activation of CO_2 at the catalyst.[87,88] However, recent computational work clearly showed that at least in some systems direct CO_2 reduction is blocked by a very high activation barrier.[38,39] For these systems bicarbonate (HCO_3^-) or carbonic acid (H_2CO_3) were identified as the most likely active species. Carbonic acid is coupled to CO_2 through a pH independent equilib-

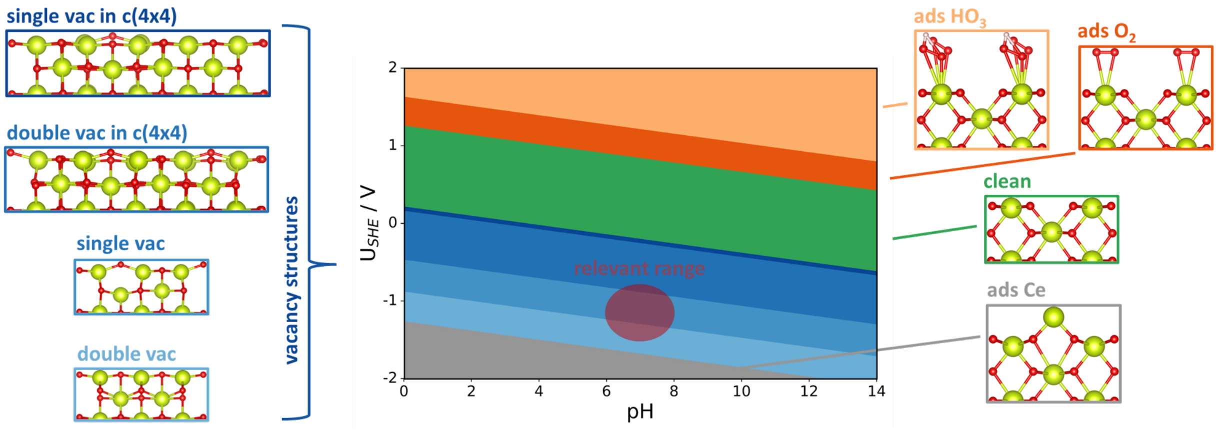

Fig. 2 Computed Pourbaix diagram of the CeO_2(110) surface. The relevant surfaces under experimental conditions are marked by the violet area. Ce: lime, H: grey and O: red.

rium.[89]

$$CO_2 + H_2O \rightleftharpoons H_2CO_3 \tag{2}$$

The formation of bicarbonate on the other hand includes the release of a single proton which renders the reaction pH dependent.[89]

$$H_2CO_3 \rightleftharpoons HCO_3{}^- + H^+ \tag{3}$$

Our computations indicate, that the formation of H_2CO_3 through reaction 2 is endergonic by 0.72 eV in DMF. Furthermore, the pK_a of carbonic acid increases from 3.88 in water[89] to 18.6 in DMF (reaction 3). The second deprotonation step has an even higher pK_a of 45.3. The trend towards significantly increased pK_a values in DMF compared to water for neutral acids is in good agreement with the significantly lower stability of protons and other charged species in aprotic non-aqueous solvents.[81,82,90] Overall, this clearly shows that only CO_2 is a possible reactant for the CO_2RR in DMF.

3.2 The Active Site at CeO_2

Under ambient conditions ceria (CeO_2) is the most stable form of cerium.[91,92] Experimental[93] as well as theoretical[94–96] studies agree that the stability of stoichiometric ceria surfaces decreases in the order (111)>(110)>(100) (see also SI Figure S.13). However, the (111) surface is chemically mostly inert and does not allow for the formation of oxygen defects under CO_2RR conditions (see also SI Figure S.13).[93–96] Also we did not find any adsorption of CO_2 on the defect free surface. This is opposed to the (110) surfaces which is known to have a strong tendency for oxygen defect formation.[97,98] Indeed, according to our computations a significant number of oxygen vacancies is already present at rather high potentials of the order of -0.2 V (Figure 2).[77] Moving towards the experimental onset potential of -1.15 V vs. SHE in acetonitrile up to 25% of the surface oxygens are removed. Owing to the repulsion interaction between vacancies, the most stable configuration features oxygen vacancies which are not directly adjacent (Figure 2).

Overall, we find a rather high concentration of surface oxygen vacancies of 25% of which each in principle can act as a reaction centre for CO_2 reduction. Accordingly, it is reasonable to assume that the chain growth starts at numerous spatially close oxygen vacancies simultaneously. Such a situation is most efficiently described by the rather small unit cell chosen by us which assumes 50% of the oxygen vacancies to be active reaction centres.

3.3 Reaction Mechanism

Building on the detailed analysis of the CeO_2(110) structure under reaction conditions and the identification of CO_2 as the sole reactant it is possible to explore the detailed reaction path to form carbon chains of varying length. Exploring and understanding reactions which can result in C-C bond formations is the core of organic chemistry and a huge amount of possible reactions have been discovered over the last 200 years. Accordingly, we nowadays have an excellent understanding of this chemistry.[99,100] Naturally, electrochemical routes to C-C bond formation possess some important differences compared to those typically used in synthetic organic chemistry. Probably the most important one is the fact that electrons with comparably high energy are easily available which renders any redox chemistry feasible, even if it results in less common intermediates. Owing to this, any mechanistic consideration must also include more exotic intermediates like carbon or oxygen radicals (unpaired electron at the C or O atom) or carbenes (free electron pair at C atom). Nevertheless, these differences are too minor to fundamentally change the organic chemistry of C-C bond formation. We therefore, opted to develop our initial candidate mechanisms by taking inspiration from standard reactions in organic chemistry like the Heck reaction[101], the aldol condensation[100], the pinacol reaction[100] and the Wurtz reaction.[100,102] In addition to this also a mechanism featuring an unstabilised carbene has been included. A summary of all considered mechanisms and their relation to the original organic reactions can be found in the SI (Figure S.1 to S.12).

Chain Start

The initial step of any CO_2RR mechanisms is the activation of CO_2. CeO_2(110) possesses a total of six potential adsorption sites and geometries (Figure 3). All attempts to adsorb CO_2 directly

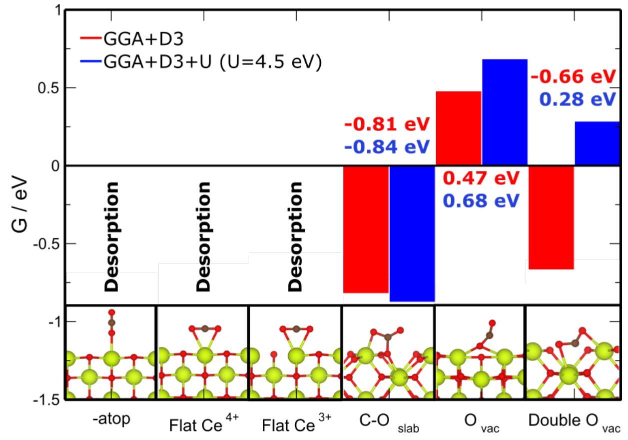

Fig. 3 Summary of CO_2 adsorption sites and Gibbs free energies of adsorption over CeO_2(110). Red bars: PBE-D3; blue bars: PBE+U-D3 (U=4.5 eV). Ce: lime, C: brown and O: red.

at either a formal Ce(III) or Ce(IV) site failed since CO_2 desorbed both when attempting to bind the molecule through carbon or oxygen. Accordingly, pinacol style (SI Figure S.4 to S.7) or Ce catalysed carbene style (SI Figure S.11 and S.12) paths can be excluded. Furthermore, carbonate and single or double oxygen vacancies remain as the only potential active sites. This agrees with the common picture of CeO_2 catalysed CO_2 reductions since high concentrations of oxygen vacancies facilitate the adsorption of CO_2.[103–105]

Let us start with the adsorption of CO_2 in a single vacancy site. This adsorption geometry is the initial step of the aldol type (SI Figure S.1 to S.3), Wurtz type (SI Figure S.8 and S.10), Heck type (SI Figure S.9 and S.10) and vacancy catalysed pinacol style type (SI Figure S.4 to S.7) paths. When binding CO_2 to this site we indeed observe the typical signs of CO_2 activation like the reduction of the O=C=O bond angle from 180° to 145° and a C–O bond length increase from 1.17 Å to 1.20 Å and 1.25 Å, respectively. The C–O bond pointing towards the surface is slightly more elongated which reflects the interactions with one of the surface Ce ions. In line with this also the Ce–O distance of 2.88 Å, compared to 2.32 Å for a bridged oxo (Ce–O–Ce) species, is still of a magnitude where some interactions can be expected. The adsorption of CO_2 into this site is somewhat endergonic by approximately 0.5 eV. It is interesting to note that this reaction becomes even more endergonic (0.7 eV) when a Hubbard U correction is added to PBE. The true value will most likely lie in between. Note that these unfavourable energetics do not necessarily result in a total inhibition of the associated reaction mechanism since the activation step in a vacancy is required to only occur once during the full mechanism. Thus, this only reduces the number of seed sites for the subsequent chain propagation.

Much more favourable energetics are observed for the adsorption if two adjacent oxygens are removed and a double vacancy is formed (up to $\Delta G = 1.2$ eV). Under these circumstances the chemisorption is exergonic by -0.7 eV for a pure GGA functional (Figure 3) while it becomes endergonic by 0.3 eV when a Hubbard U correction is added. Similar to the adsorption in a single vacancy site, also a significant activation of CO_2 is observed here. For example the C–O bond length is elongated to 1.26 Å and 1.31 Å while the O=C=O bond angle is at the same time reduced from 180° to only 125°. This adsorption geometry is accompanied by some interactions between the carbon and the adjacent Ce ion as indicated by the rather short Ce···CO_2 distance of 2.67 Å. However, the formation of adjacent oxygen vacancies is thermodynamically unfavourable (see SI) which renders this adsorption geometry unlikely.

The last stable CO_2 adsorption mode is the adsorption at a surface oxygen which results in the formation of a surface carbonate. This path comprises the starting point for another pinacol style path. This reaction is with -0.8 eV thermodynamically even more favourable than the adsorption in a double vacancy (Figure 3). A comparable value is also obtained with GGA+U. Identical to the two alternative adsorption modes also CO_2 bound in this fashion displays the typical signs of activation. E.g. the O–C–O bond angle is reduced to 126° while the C–O bond lengths are increased to 1.28 Å for the CO units pointing outwards and 1.35 Å for the CO unit pointing towards CeO_2. In line with the adsorbate's apparent carbonate character we also find very strong interactions with the adjacent Ce ions as indicated by the rather short Ce–O bond lengths of the order of 2.41 Å to 2.56 Å which compares favourably to a typical Ce–O–Ce single bond of 2.32 Å.

This structure can be converted electrochemically under water elimination to CO_2 in two consecutive PCET reduction steps (reactions 4 and 5).

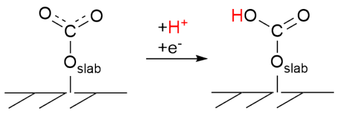

(4)

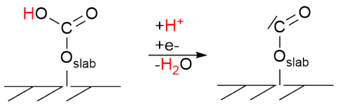

(5)

The product of this reduction reaction is structurally identical to a single vacancy adsorbed CO_2. The first PCET step of the reduction mechanism (reaction 4) occurs a potential of 0.0 V vs. SHE. This is opposed to the subsequent reductive elimination (reaction 5) which requires a very negative potential of -1.5 V. This potential is slightly higher than the experimental onset potential[51] but still falls within the expected order of magnitude considering the error bars associated with our computations. Interestingly, we were only able to stabilize the vacancy adsorbed CO_2 by putting CO_2 directly at the surface while we observed its desorption when attempting to converge the structures coming from the carbonate intermediate. This could be indicative of a rather minor barrier which in turn would result in a fast equilibrium between dissolved and vacancy adsorbed CO_2.

Chain Propagation

Once CO_2 has adsorbed at the surface, the chain can grow by reacting with additional CO or CO_2. As discussed above, the formation of surface carbonates comprises a highly favourable and likely intermediate. In terms of chain propagation, it is the starting point for a pinacol style C-C coupling reaction between two

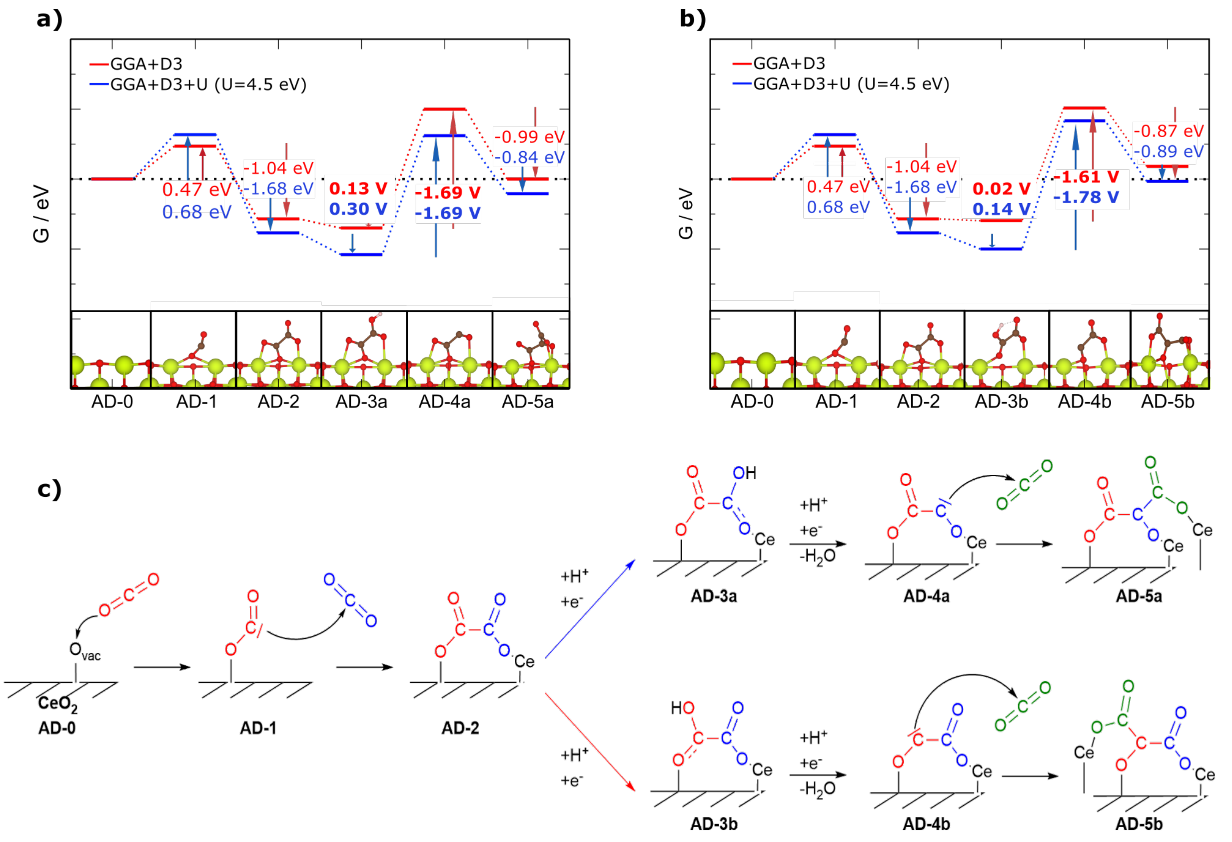

Fig. 4 a) Gibbs Free energies of the initialization and chain propagation steps through the carbon not directly bound to the surface (path a). Red lines: PBE-D3; blue lines: PBE+U-D3 (U=4.5 eV) b) Gibbs Free energies of the initialization and chain propagation steps through the carbon directly bound to the surface (path b). Red lines: PBE-D3; blue lines: PBE+U-D3 (U=4.5 eV) c) Schematic mechanism for the initialization and chain propagation steps. Ce: lime, C: brown, O: red and H: grey.

adjacent surface carbonates. Our computations indicate, that this mechanism is unlikely since no formation of a stable C-C bond could be achieved. This is indeed not surprising when considering, that carbonates are chemically inert and do not posses a free electron pair at the carbon which is a prerequisite for this reaction.

Thus, only single vacancy bound CO_2 is a reasonable starting point. This leaves aldol, Wurtz, Heck or vacancy catalysed pinacol style reactions as possible routes for hard carbon formation. A Wurtz style reaction can be excluded immediately since this path would require the presence of two adjacent CO_2 molecules adsorbed at oxygen vacancy sites (see SI, Figure S.9 for details). This vacancy configuration is, according to our computations, energetically unfavourable (see SI). Accordingly, also the presence of two adjacent CO_2 is unlikely. Naturally, this also excludes a vacancy catalysed pinacol style reaction which has a similar structural requirement. Furthermore, we do not find any stable configuration for a Heck style coupling of a dissolved CO_2 with a vacancy bound CO_2. This is indeed not surprising when considering, that C−Ce bonds in CeO_2 are unstable owing to the high oxophilicity of Ce.[89,106]

Accordingly, only the aldol condensation type mechanism remains as possible reaction path. A summary of the initial steps for C-C bond formation assuming CO_2 as reactant and the subsequent chain propagation is shown in Figure 4. C-C bond formation is achieved through the reaction of a vacancy adsorbed CO_2 with a dissolved CO_2 (see also reaction from AD-1 to AD-2 in Figure 4).

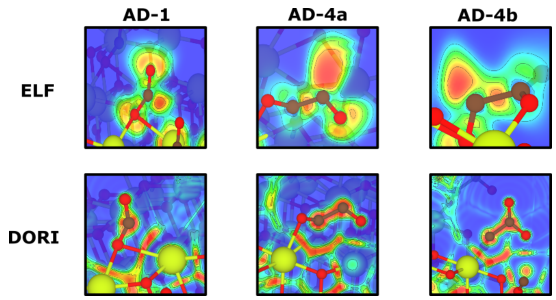

Fig. 5 Density overlap region indicator (DORI) and electron localisation plots (ELF) of central intermediates are depicted. Ce: lime, C: brown and O: red.

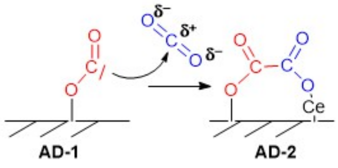

(6)

This step is strongly exergonic by approximately -1.0 eV (PBE-

D3) and -1.7 eV (PBE+U-D3) which renders it thermodynamically highly favourable (Figure 4). The very high gain in energy can be understood from a detailed analysis of the electronic structure of AD-1. At first glance, this intermediate has significant similarities to an ordinary carboxylate (R$-$COO$^-$) group. E.g. it consists of a carbon with formally three bonds to two oxygen atoms. For a normal CO_2RR, this structure would be stabilized by a fourth bond to a metal centre.[38,39,46,62] However, in the present case the C-Ce distance of 2.88 Å indicates the absence of a strong covalent bond. This is also confirmed by the density overlap region indicator (DORI; Figure 5a) and electron localization function (ELF; Figure 5a) plots. The former is characterized by the absence of a localized basin between Ce and C which is a clear sign of the absence of a covalent bond between both atoms.[73,107] Furthermore, ELF indicates the presence of a localized electron pair at the carbon atom. This is also confirmed by the partial density of states (PDOS) which only show signs of a weak π-complex which interacts through the C=O double bond with Ce. This is indicated by the overlap of the O, C and Ce bands close to the Fermi level (Figure 6a). The interacting orbital is only occupied by a single α-spin electron which renders it at least a partial radical. However, the corresponding unoccupied β-spin orbital is energetically very close. Thus, this orbital can easily become occupied when applying an electrochemical potential of less than -1.0 V vs. SHE through an electron transfer from bulk CeO_2.

Note that both states are, even in the absence of an electrochemical potential, possible resonance structures. Chemically speaking, this state corresponds to a poorly stabilized carbene or carbon radical which is characterized by a free electron or electron pair at the carbon. These intermediates are highly reactive[100] which is in line with the observed very exergonic reaction energy. In what follows we will, for the sake of simplicity, refer to reactive carbons of this or similar electronic structure as "carbenes".

The purely chemical C-C bond formation is followed by the stepwise electrochemical reduction of the C=O unit (AD-2 to AD-3a or AD-3b in Figure 4) and its elimination as water (AD-3a/AD-3b to AD-4a/AD-4b in Figure 4). Hydrogenation and water elimination may either occur at C_1 (CO_2 group anchored in the CeO_2 oxygen vacancy; lower path in Figure 4c) or C_2 (newly attached CO_2 group; upper path in Figure 4c). The first reduction step occurs in both cases already at a slightly positive potential between 0.0 V and 0.1 V vs. SHE and is therefore unproblematic at the potentials applied for CO_2 reduction (Figure 4). Comparable energetics are also obtained with GGA+U. The subsequent water elimination step on the other hand requires in both cases a very negative potential of approximately -1.7 V vs. SHE which corresponds to the lowest redox potential observed in the reaction mechanism. Thus, at least a potential of this magnitude must be applied to allow all electrochemical steps to proceed, i.e. this reaction is potential determining (for details see SI equation 8).[62,108,109]

At this potential water would also be reduced to hydrogen. However, even in water (pH 7), the onset for hydrogen evolution over CeO_2 is of the order of approximately -1.3 V vs. SHE.[110] Furthermore, the reaction is performed in DMF with minor amounts of water.[51] Accordingly, this side reaction is at least to some degree suppressed. The presence of this very negative reduction potential is not unexpected when considering the products' detailed electronic structure which is similar to the carbene in AD-1. Identical to this structure we also observe for AD-4a and AD-4b the typical signs of a highly reactive carbon radical and/or carbene in the ELF (Figure 5b and c). Additional support for this interpretation is also found in the PDOS plots (Figure 6b and c). Note that for AD-4b again some indications for weak interactions with Ce are present which points towards a weak π-complex type interaction. However, no indications for a strong covalent C$-$Ce bond is observed in the DORI plot (Figure 5b and c). No indications for comparable interactions are observed for AD-4a. Almost identical energetics are also obtained when applying a Hubbard U to Ce.

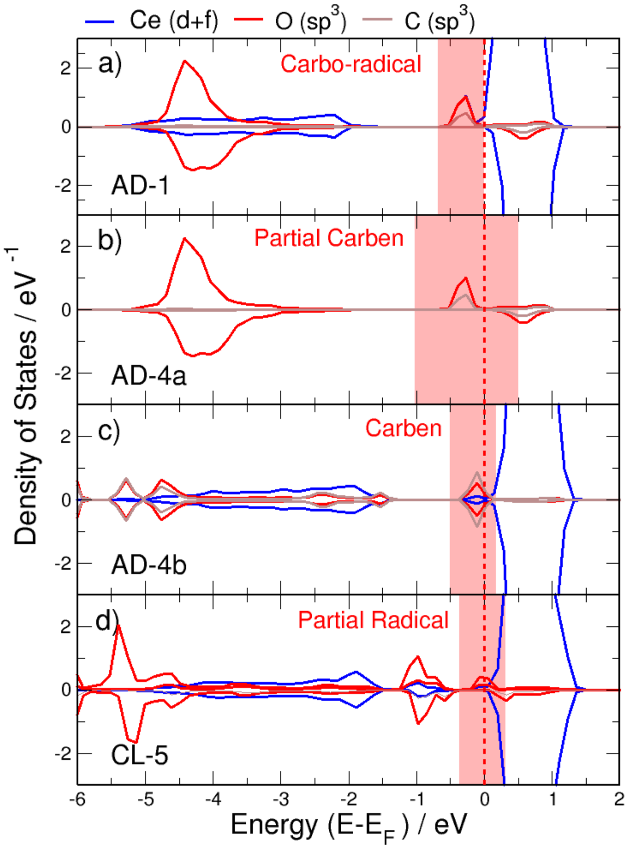

Fig. 6 Spin-polarized PDOS-plots of the crucial CO_2RR intermediates.

Note that the onset potential predicted by us is with -1.7 V vs. SHE significantly larger than the -1.15 V vs. SHE found by Esrafilzadeh et al.[51] However, it must be cautioned that the authors decided to report an onset potential at which almost no current density is observed rather than following the more common approach to report an overpotential to reach a defined current density.[111,112] Indeed, the current density remains far below 1 mA/cm^2 until a much lower potential of roughly -1.8 V vs. SHE is reached. In addition to this our computations also do not include solvation effects which would stabilize the eliminated water molecule by -0.24 eV (Gaussian16/M06-2X/SMD) compared to our gas phase reference. This in turn would shift the onset potential towards a less negative value. Furthermore, protons are destabilized by approximately 0.7 eV in DMF compared to water.[81,82] Including these effects would increase the onset potential to a value of approximately -0.9 V. An additional source of uncertainties is the possible presence of Ag impurities in the electrolyte which are known to leak from the "leakless" Ag^+/Ag-reference electrode[113] used by Esrafilzadeh et al.[51] A leak of Ag^+ ions or even Ag nanoparticles could stabilize the undercoordinated carbon which would lower the onset potential further. Indeed, C−Ag bonds are well known motives in organometallic chemistry.[106] This beneficial contribution of trace amounts of impurities is not uncommon and has been observed in many other cases.[76,113–115] Such a mechanism would also be in good agreement with the observed very low current density at lower overpotentials which in this case would effectively be limited by the amount of available silver and its diffusion to the electrode.

Once the carbene species in AD-4a or AD-4b has been formed, C−C bond formation through a nucleophilic attack at a dissolved CO_2 atom takes place. This allows the chain to grow by an additional C_1 unit. In line with the very high reactivity of a carbene species, this step is strongly exergonic by roughly -0.9 eV for both pure GGA and GGA+U independent of whether CO_2 is attacked from a carbene at C_1 or C_2. From here the polymerization mechanism proceeds by repeating the previous steps. E.g. a reactive carbene intermediate is formed through the reduction of a C=O unit and water elimination followed by its attack on a dissolved CO_2.

Overall, the proposed mechanism requires CeO_2 only as an anchor for the initial adsorption of the first CO_2. Beyond this point, the reaction becomes surprisingly independent from the catalyst. Accordingly, also later oligo- and polymerization steps can proceed without the need for interactions with the catalyst provided an electron transfer from the cathode to the terminating carboxylate (R−COO) group is feasible and CO_2 is still available as feedstock. Once the chain has grown through subsequent reactions with CO_2, also the reduction and conversion of the keto group into their enol form becomes possible. This results in the formation of an energetically favourable conjugated π-electron system. The obtained conjugated π-electron system allows for the stabilisation of the carbene which in turn makes subsequent water elimination steps energetically even more favourable.

An important variation of the above mechanism is to assume CO as feedstock. CO may for example be formed in-situ through reduction of CO_2. In this case the chain growth becomes purely chemical. E.g. the only required reaction steps are the nucleophilic attack of the carbene at a dissolved CO. In contrast to the attack on CO_2, this reaction is only thermoneutral. This is not unexpected when considering that the highest occupied molecular orbital (HOMO) in CO is a carbon centred σ^* anti-bonding orbital which places significant electron density at the carbon.[106,116] Accordingly, CO is a very poor electrophile. Indeed, chain propagation through reactions with CO typically proceeds through a migratory insertion in which CO binds to the catalyst prior to forming a C-C bond (reaction 7).[106]

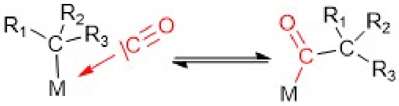

(7)

In the present case no such interaction with the catalyst is possible owing to the oxophilicity of Ce and the steric constraints of the Ce centres for which all free valences are already saturated. This renders such a variation of the mechanism highly unlikely.

Chain Linkage

The chains formed during the propagation steps may at some point meet and link with other olefine chains. To evaluate possible chain linkage mechanisms a model system whose unit cell was doubled along the x-axis was constructed (see Figure 1). This reduces the strain within the olefine chain and thus, corresponds to a more realistic situation. Furthermore, all keto groups were reduced to their enol form since this allows for the formation of a long and energetically favourable conjugated π electron system.

Identical to the previous chain propagation steps also the chain linkage is initialized by the reduction of two terminal R−COO· groups to two carbonic acids (R−COOH; reaction from CL-1 to CL-3 in Figure 7a). Both reaction steps are energetically highly favourable as indicated by the rather high reduction potentials of -0.2 V and 0.7 V vs. SHE (Figure 8). Note that during the second step a proton transfer from the R−COOH group to a surface Ce−O−Ce oxo site occurs. This allows for a much more stable configuration and thus, results in a positive potential for the second reduction reaction. Overall, both steps are unproblematic under reaction conditions. The subsequent reductive elimination through release of water (reaction from CL-3 to CL-5 in Figure 7) is thermodynamically significantly more demanding as indicated by the very negative potential of -1.8 V vs. SHE for the first water elimination. This value is comparable to what has been observed for earlier water elimination steps (compare with Figure 4). The slight decrease of the potential by approximately -0.2 V might be the result of having to break a rather strong hydrogen bond (d(HO···HO)=1.78 Å) between the carboxylic acid OH group and an adjacent alcohol. As a part of this elimination step also the opposite carboxylic acid group rearranges by transferring the proton back from the surface Ce−OH−Ce group to the $R{-}COO^-$ group. In addition to this also a strong hydrogen bond between the OH group of the carboxylic acid and an alcohol at the opposite chain is formed (d(HO···HO)=1.65 Å). The second water elimination in contrast occurs already at a much higher potential of only 0.1 V vs. SHE.

In principle chain linkage could now proceed through a simple CO_2 insertion. However, our computations show that this reaction is thermodynamically unfavourable. E.g. the direct chain linkage is endergonic by 1.5 eV. At first glance, this may seem surprising when comparing it to the very exergonic C−C bond formation steps during the chain propagation phase. However, this result can be rationalized by the marked differences in the electronic structure. The first and probably most important difference is the fact that the newly inserted carbon atom possesses

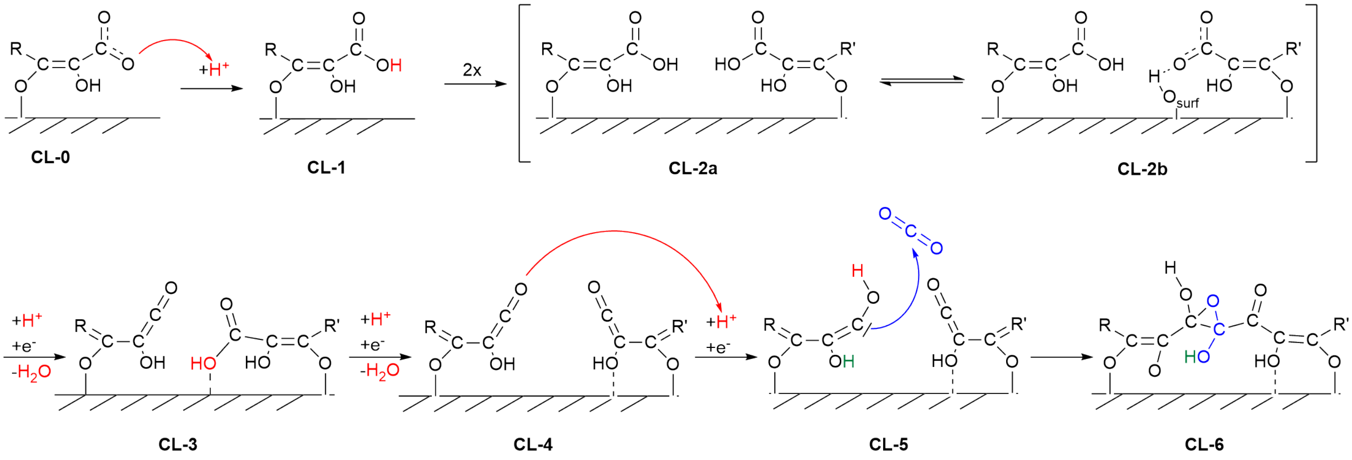

Fig. 7 Schematic summary of the most likely reaction mechanism for the linkage of two olefine chains.

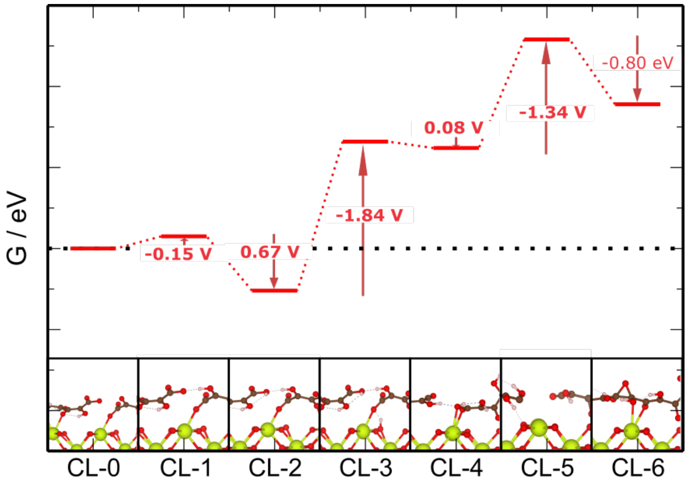

Fig. 8 Energetics of the chain linkage mechanism. For the detailed mechanism see Figure 7. The reaction energies were obtained using a pure PBE-D3 functional. Ce: lime, C: brown, O: red and H: grey.

an sp^3 hybridization and thus, is not part of a delocalized π electron system. Accordingly, two formal radical C–O· groups are obtained. One of these groups is stabilized through a proton transfer from an adjacent alcohol which itself is oxidized to a ketone. In addition to this, the chain rearranges such, that the C–OH bond is weakened (bond elongation from 1.31 Å for an alcohol to 1.58 Å). This configuration is stabilized by a Ce–OH interaction (d(Ce-O)=2.53 Å) and a strong hydrogen bond to the second adjacent alcoholic group (d(HO···HO)=1.53 Å). This allows the second C–O· radical to form at least a partial C=O double bond (see SI). However, the very long C–O bond length of 1.30 Å, which is close to the bond length observed for an alcohol, suggests that the oxygen is still mostly of radical nature.

In addition to this, the terminal C_2O groups form linear ketene derivatives ($R_2C{=}C{=}O$) where one of the C–R bonds correspond to the enol chain and the second R to an OH group. While ketenes themselves are highly reactive[99,100,117] they generally react as electrophiles, e.g. they accept an electron pair.[118] No such reaction is possible with CO_2 which is, owing to the very stable C=O double bonds, unable to provide an electron pair. This is opposed to CO which can donate its lone pair to form C–C bonds with both ketene groups and thus, link both chains. In addition to this, the inserted CO forms a ketone rather than an unstable "double radical". In line with this, CO insertion is energetically extremely favourable by -5.2 eV. Note that this very strong exergonicity is not unexpected since CO is inserted between two extremely reactive functional groups under formation of two new C–C bonds.

A more likely reaction route in the absence of CO would be chain linkage through a [2+2] cyclo-addition of two ketenes which mostly results in the formation of 4-membered cyclic esters (β-Lactones; reaction 8).[99,119–124]

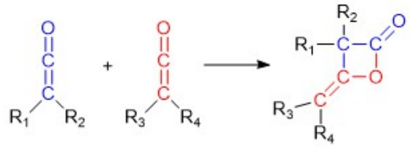

(8)

This ester could in turn be converted into an olefine through a simple ester hydrolysis (reaction 9).

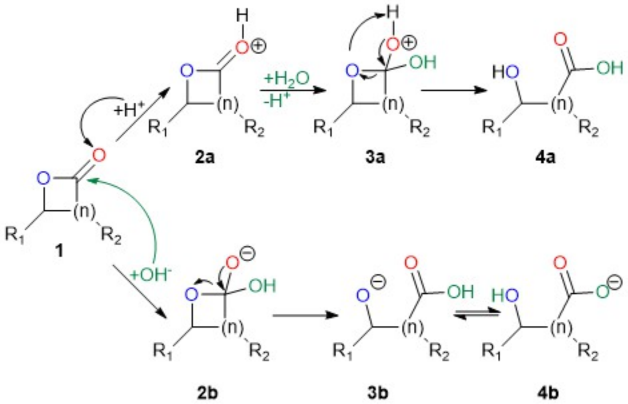

(9)

For many ketenes such a reaction can already proceed at room temperature.[99,100,117,119,120] A similar [2+2] cyclo-additions between ketenes and CO_2 is in principle possible under elevated temperature or irradiation but typically too slow to be of relevance for chain propagation or chain linkage.[125]

These reactions are, owing to the limited flexibility of our model system, impossible in the present case. Instead, the ketene

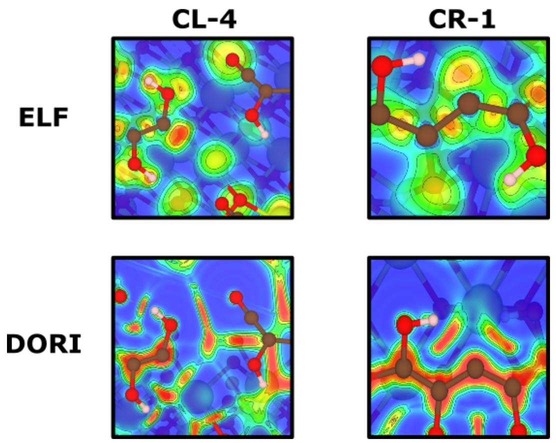

Fig. 9 Density overlap region indicator (DORI) and electron localisation plots (ELF) of central ketene intermediates CL-5 and CR-1 in Figure 7 and Figure 10. Ce: lime, C: brown, O: red and H: grey.

is reduced to a R_2−C=C−OH species at a rather negative potential of -1.34 V vs. SHE (CL-4 to CL-5 in Figure 7). This converts the terminal carbon again into a highly reactive intermediate. According to the PDOS (Figure 6d), it is, similar to the initial carbene of AD-1, characterized by a singly occupied C−O with the unoccupied β spin being very close in energy. In line with this we observe the usual characteristics of a free electron or electron pair in the ELF (see Figure 9). According to the DORI and the PDOS this carbene seems to be somewhat stabilized through interactions with Ce (see Figure 9 and 6d). Thus, the electronic structure is again best described by a superposition of the radical and carbene mesomeric structures . The obtained carbene is finally sufficiently reactive to allow for the insertion of CO_2 through a nucleophilic attack (reaction 10).

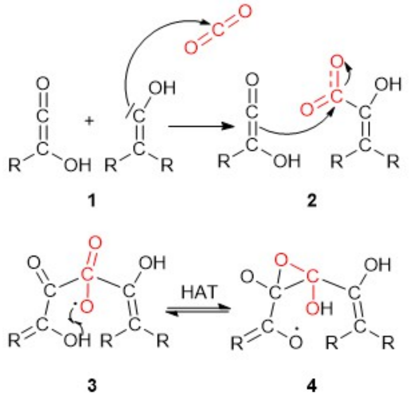

(10)

This step is rather strongly exergonic by -0.80 eV (Figure 8). As a part of this reaction a hydrogen is transferred from an adjacent alcohol which in turn is oxidized to a ketone. In addition to this, the second C−O· radical stabilizes itself by forming an epoxide with the adjacent carbon atom (reaction 10). Breaking the epoxide electrochemically is a well established reaction[126,127] for which no major barriers are expected.

Overall, chain linkage requires a comparable onset potential as the general chain propagation reactions and is therefore energetically feasible if the initial propagation steps can occur.

Chain Branching

In addition to the linkage of chains also building connections between independently growing polymers is a necessary requirement for the formation of carbonaceous materials or hard carbon. The linkage of independent chains or the formation of cyclopentadiene (5-membered unsaturated rings) or benzene rings (6-membered unsaturated rings) can also proceed through an equivalent electrochemical aldol condensation type mechanism. The reaction is exemplified by considering the formation of a cyclopentadiene ring from a fully conjugated enol chain as precursor (Figure 10). Attempts to form 6-membered rings failed owing to the very high tendency of ketenes for ring closure. However, numerous reactions for ring expansion which could increase the ring size from a 5-membered to a 6-membered ring are known in organic chemistry.[99,128] Furthermore, the restriction to a 5-membered ring is the result of the rather special reaction steps considered by us which assumes the simultaneous formation of side chains in early stages. For example the linkage of longer side chains through formation of a carbene followed by insertion of CO_2 would directly result in the formation of a 6-membered ring. Studying all possible reactions is, however, highly complex and therefore far beyond the scope of this contribution.

Identical to the previously discussed steps also chain branching is initialized by the elimination of one of the OH groups as water to form a carbene. This reaction can proceed through a purely chemical step which involves a hydrogen atom transfer from one of the adjacent alcohol groups (CR-0 to CR-1 in Figure 10). This reaction is moderately exergonic by -0.4 eV (Figure 11). The surprisingly favourable energetics are a direct result of the possibility to delocalize the otherwise highly reactive free electron pair at the carbene through a long conjugated π electron system and the newly formed ketone. Additionally, there is also a localized basin between the hydrogen of the adjacent alcohol and the carbene in the DORI (Figure 9). This indicates the presence of a strong hydrogen bond which stabilizes the free electron pair further. In line with this we also observe a rather short COH···C distance of 1.92 Å. Besides the chemical path also an electrochemical water elimination is possible. This reaction is also energetically favourable and requires a positive potential of 0.1 V vs. SHE.

Once the carbene has been formed, C-C bond formation is achieved through a nucleophilic attack at a dissolved CO_2 (CR-2 to CR-3 in Figure 10). Assuming a direct attack without prior reduction of the newly formed keto group, this step is moderately exergonic by -0.4 eV (Figure 11). However, also the competing reduction of the newly formed ketone is thermodynamically highly favourable under experimental conditions since it occurs already at a rather positive potential of 0.2 V vs. SHE(Figure 11). If this reduction takes place prior to the nucleophilic attack than C-C bond formation becomes strongly exergonic by -1.8 eV (Figure 11).

C-C bond formation is followed by the reduction of the hydrogenation of the R−COO group to form a carbonic acid (R−COOH) and water elimination. The former step requires a potential of approximately 0.0 V vs. SHE (CR-3 to CR-4 in Figure 11) which renders it thermodynamically favourable. The water elimination

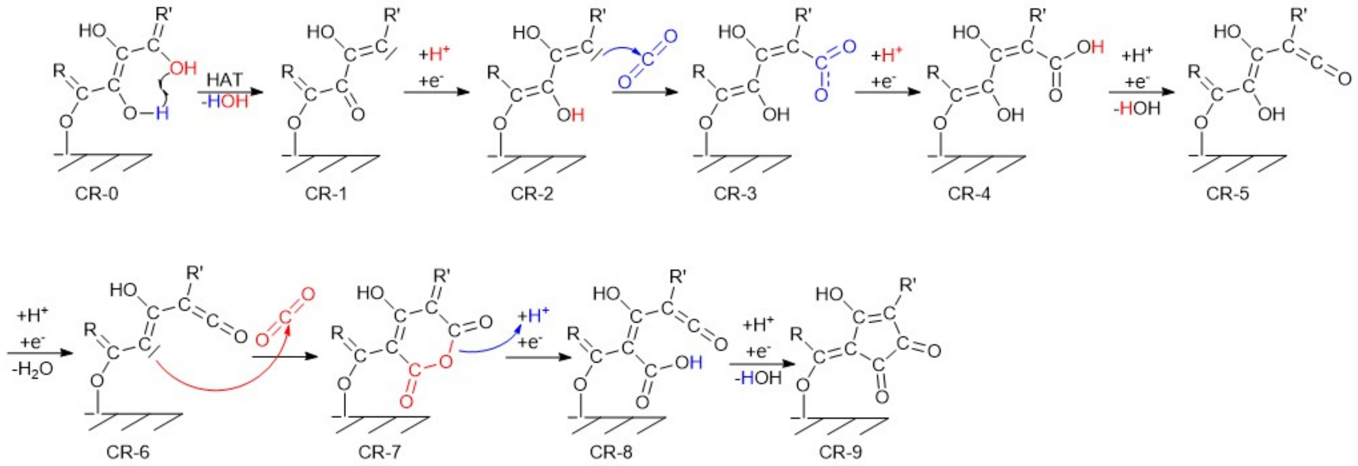

Fig. 10 Summary of an example reaction mechanism for the formation of side chains.

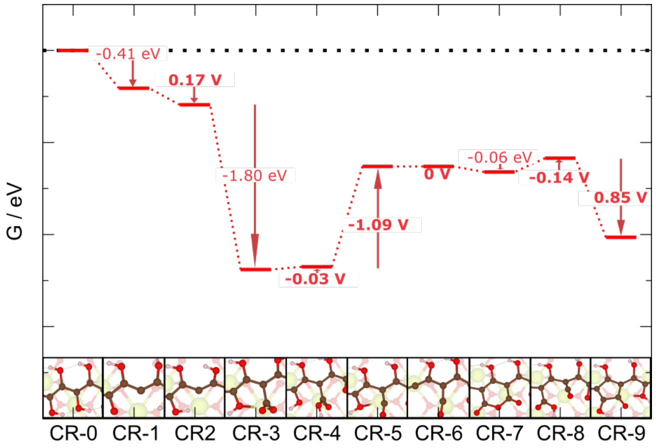

Fig. 11 Energetics of the example mechanism for the branching of the olefine chain. Ce: lime, C: brown, O: red and H: grey.

step to form a ketene on the other hand requires a much more negative potential of -1.1 V vs. SHE which can still be overcome under CO_2RR conditions (CR-4 to CR-5 in Figure 11). Following the ketene formation the side chain can grow, identical to the chain propagation mechanism, through an electrochemical aldol condensation (compare to Figure 4). Considering the repetitive nature of this polymerization mechanism it is reasonable to assume that all subsequent steps require energies similar to the chain propagation steps (Figure 4).

An interesting side reaction is observed in the presence of an adjacent ketone. Here, water elimination does not lead to the formation of a ketene but rather results in the direct formation of an unsaturated γ-lactone (5-membered cyclic ester; reaction 11).

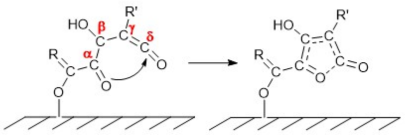

(11)

Thanks to the ester formation this reaction is energetically highly favourable and occurs already at a very positive potential of 1.0 V vs. SHE. The lactone can be split through a simple ester hydrolysis[100,129,130] and therefore does not constitute a dead end.

Naturally, also a second chain can start to grow in the vicinity through an additional elimination of an alcohol (CR-5 to CR-6 in Figure 10). Assuming an electrochemical water elimination step, this reaction occurs already at a potential of 0.0 V vs. SHE. The subsequent C−C bond formation is then roughly thermoneutral (ΔG=-0.1 eV) and results in the direct formation of a Glutaconic anhydride derivative (6-membered cyclic anhydride; CR-6 to CR-7 in Figure 10). This reaction is not unexpected considering that the formed carboxylate is a fair nucleophile and ketenes are highly susceptible to nucleophilic attacks.

The anhydride is easily split electrochemically at a potential of -0.1 V vs. SHE. This results in the formation of a carbonic acid and a ketene CR-7 to CR-8 in Figure 10). Eliminating the OH group of the carbonic acid finally initiates a concerted reaction step in which water is eliminated and a cyclopent-3-ene-1,2-dione derivative is formed formed (cyclic 5-membered ring with two keto groups; CR-8 to CR-9 in Figure 10). The overall reaction is energetically highly favourable and thus, possible at the electrode potential applied in experiment.[51]

4 Conclusions

Inspired by well established reactions in organic chemistry we have evaluated the reaction mechanisms for CO_2 reduction over CeO_2(110). According to our computations the reaction is initialized by the adsorption of CO_2 into an oxygen vacancy site. Owing to the rich defect chemistry of ceria suitable sites are ample. This renders the initial CO_2 adsorption step feasible despite being endergonic. C-C bond formation is then achieved through an aldol condensation type mechanism in which a carbene intermediate performs a nucleophilic attack on CO_2. This is followed by the formation of a new carbene through electrochemical elimination of water. Interestingly, only the initial adsorption step is strongly affected by ceria while all other steps appear to be almost completely independent from the catalyst. This mechanism is completely generic and can be repeated for all steps of the polymerization of CO_2. This fundamental mechanistic understanding lays the foundation for the development of enhanced catalysts for the conversion of CO_2 to hard carbon and may also help to develop new routes for electrosynthesis of organic compounds.

Conflicts of interest

There are no conflicts to declare.

Acknowledgements

F.K. and J.D. acknowledge funding through the German Bundesministerium für Bildung and Forschung (BMBF) project NETPEC (grant number: No. 01LS2103A). M.B. is grateful for financial support from the Dr. Barbara-Mez-Starck foundation. Computer time provided by the state of Baden-Württemberg through bwHPC and the German Research Foundation (DFG) through grant no INST 40/575-1 FUGG (JUSTUS 2 cluster) is gratefully acknowledged.

Notes and references

1 P. Friedlingstein, M. O'Sullivan, M. W. Jones, R. M. Andrew, L. Gregor, J. Hauck, C. L. Quéré, I. T. Luijkx, A. Olsen, G. P. Peters, W. Peters, J. Pongratz, C. Schwingshackl, S. Sitch, J. G. Canadell, P. Ciais, R. B. Jackson, S. R. Alin, R. Alkama, A. Arneth, V. K. Arora, N. R. Bates, M. Becker, N. Bellouin, H. C. Bittig, L. Bopp, F. Chevallier, L. P. Chini, M. Cronin, W. Evans, S. Falk, R. A. Feely, T. Gasser, M. Gehlen, T. Gkritzalis, L. Gloege, G. Grassi, N. Gruber, Özgür Gürses, I. Harris, M. Hefner, R. A. Houghton, G. C. Hurtt, Y. Iida, T. Ilyina, A. K. Jain, A. Jersild, K. Kadono, E. Kato, D. Kennedy, K. K. Goldewijk, J. Knauer, J. I. Korsbakken, P. Landschützer, N. Lefèvre, K. Lindsay, J. Liu, Z. Liu, G. Marland, N. Mayot, M. J. McGrath, N. Metzl, N. M. Monacci, D. R. Munro, S.-I. Nakaoka, Y. Niwa, K. O'Brien, T. Ono, P. I. Palmer, N. Pan, D. Pierrot, K. Pocock, B. Poulter, L. Resplandy, E. Robertson, C. Rödenbeck, C. Rodriguez, T. M. Rosan, J. Schwinger, R. Séférian, J. D. Shutler, I. Skjelvan, T. Steinhoff, Q. Sun, A. J. Sutton, C. Sweeney, S. Takao, T. Tanhua, P. P. Tans, X. Tian, H. Tian, B. Tilbrook, H. Tsujino, F. Tubiello, G. R. van der Werf, A. P. Walker, R. Wanninkhof, C. Whitehead, A. W. Wranne, R. Wright, W. Yuan, C. Yue, X. Yue, S. Zaehle, J. Zeng and B. Zheng, *Earth Syst. Sci. Data*, 2022, **14**, 4811–4900.

2 D. Lüthi, M. L. Floch, B. Bereiter, T. Blunier, J.-M. Barnola, U. Siegenthaler, D. Raynaud, J. Jouzel, H. Fischer, K. Kawamura and T. F. Stocker, *Nature*, 2008, **453**, 379–382.

3 G. H. Rau, *Nature Climate Change*, 2019, **9**, 256–256.

4 M. M. May and K. Rehfeld, *Adv. Energy Mater.*, 2022, **12**, 2103801.

5 S. Erşan and J. O. Park, *Joule*, 2020, **4**, 2047–2051.

6 H. Onyeaka, T. Miri, K. Obileke, A. Hart, C. Anumudu and Z. T. Al-Sharify, *Carbon Capture Sci. Technol.*, 2021, **1**, 100007.

7 P. Gabrielli, M. Gazzani and M. Mazzotti, *Ind. Eng. Chem. Res.*, 2020, **59**, 7033–7045.

8 D. Lefebvre, A. G. Williams, G. J. D. Kirk, Paul, J. Burgess, J. Meersmans, M. R. Silman, F. Román-Dañobeytia, J. Farfan and P. Smith, *Sci. Rep.*, 2021, **11**, 19907.

9 P. Kelemen, S. M. Benson, H. Pilorgé, P. Psarras and J. Wilcox, *Front. Clim.*, 2019, **1**, 9.

10 P. Saha, S. Amanullah and A. Dey, *Acc. Chem. Res.*, 2022-01, **55**, 134–144.

11 H. S. Shafaat and J. Y. Yang, *Nature Catalysis*, 2021, **4**, 928–933.

12 S. Overa, B. H. Ko, Y. Zhao and F. Jiao, *Acc. Chem. Res.*, 2022, **55**, 638–648.

13 A. R. Paris and A. B. Bocarsly, *ACS Catal.*, 2019, **9**, 2324–2333.

14 E. Schuler, M. Demetriou, N. R. Shiju and G.-J. M. Gruter, *ChemSusChem*, 2021, **14**, 3636–3664.

15 J. Ren, F.-F. Li, J. Lau, L. González-Urbina and S. Licht, *Nano Lett.*, 2015-08, **15**, 6142–6148.

16 L. Pastero, N. Curetti, M. A. Ortenzi, M. Schiavoni, E. Destefanis and A. Pavese, *Sci Total Environ*, 2019, **666**, 1232–1244.

17 R. Angamuthu, P. Byers, M. Lutz, A. L. Spek and E. Bouwman, *Science*, 2010, **327**, 313–315.

18 F. P. G. de Arquer, C.-T. Dinh, A. Ozden, J. Wicks, C. McCallum, A. R. Kirmani, D.-H. Nam, C. Gabardo, A. Seifitokaldani, X. Wang, Y. C. Li, F. Li, J. Edwards, L. J. Richter, S. J. Thorpe, D. Sinton and E. H. Sargent, *Science*, 2020, **367**, 661–666.

19 H. Ritchie, M. Roser and P. Rosado, *Our World in Data*, 2020.

20 N. MacDowell, N. Florin, A. Buchard, J. Hallett, A. Galindo, G. Jackson, C. S. Adjiman, C. K. Williams, N. Shah and P. Fennell, *Energy Environ. Sci.*, 2010, **3**, 1645.

21 S. Bouzalakos and M. Mercedes, in *Developments and Innovation in Carbon Dioxide (CO2) Capture and Storage Technology*, Elsevier, 2010, pp. 1–24.

22 I. Melián-Cabrera, M. L. Granados and J. Fierro, *Catal. Lett.*, 2002, **79**, 165–170.

23 I. Melián-Cabrera, M. L. Granados and J. Fierro, *J. Catal.*, 2002, **210**, 273–284.

24 M. Bowker, *ChemCatChem*, 2019, **11**, 4238–4246.

25 A. Posada-Borbón and H. Grönbeck, *ACS Catal.*, 2021, **11**, 9996–10006.

26 R. Francke, B. Schille and M. Roemelt, *Chem. Rev.*, 2018, **118**, 4631–4701.

27 M. R. Dubois and D. L. Dubois, *Acc. Chem. Res.*, 2009, **42**, 1974–1982.

28 J. Hawecker, J.-M. Lehn and R. Ziessel, *J. Chem. Soc., Chem. Commun.*, 1984, 328–330.

29 B. P. Sullivan, C. M. Bolinger, D. Conrad, W. J. Vining and T. J. Meyer, *J. Chem. Soc., Chem. Commun.*, 1985, 1414–1416.

30 S. Zhang, Q. Fan, R. Xia and T. J. Meyer, *Acc. Chem. Res.*, 2020, **53**, 255–264.

31 S. Zhang, P. Kang, M. Bakir, A. M. Lapides, C. J. Dares and T. J. Meyer, *Proc. Natl. Acad. Sci. U.S.A.*, 2015-12, **112**, 15809–15814.

32 Y. Wang, D. Wang, C. J. Dares, S. L. Marquard, M. V. Sheri-

dan and T. J. Meyer, *Proc. Natl. Acad. Sci. U.S.A.*, 2017-12, **115**, 278–283.

33 S. Kaneco, H. Katsumata, T. Suzuki and K. Ohta, *Electrochim. Acta*, 2006, **51**, 3316–3321.

34 C. Cometto, L. Chen, P. Lo, Z. Guo, K. Lau, E. Anxolabehere-Mallart, C. Fave, T. Lau and M. Robert, *ACS Catal.*, 2018, **8**, 3411–3417.

35 C. Cometto, L. Chen, D. Mendoza, B. Lassalle-Kaiser, T. Lau and M. Robert, *ChemSusChem*, 2019, **12**, 4500–4505.

36 C. Costentin, S. Drouet, M. Robert and J. Savéant, *Science*, 2012, **338**, 90–94.

37 J. Shen, R. Kortlever, R. Kas, Y. Birdja, O. Diaz-Morales, Y. Kwon, I. Ledezma-Yanez, K. Schouten, G. Mul and M. Koper, *Nature Commun.*, 2015, **6**, 8177–.

38 R. Khakpour, D. Lindberg, K. Laasonen and M. Busch, *ChemCatChem*, 2023, **15**, e2022016.

39 R. Khakpour, K. Laasonen and M. Busch, *Electrochim. Acta*, 2023, **442**, 141784.

40 A. Göttle and M. Koper, *J. Am. Chem. Soc.*, 2018, **140**, 4826–4834.

41 M. N. Hossain, R. Khakpour, M. Busch, M. Suominen, K. Laasonen and T. Kallio, *ACS Appl. Energy Mater.*, 2022-12, **6**, 267–277.

42 S.-T. Dong, C. Xu and B. Lassalle-Kaiser, *Chem. Sci.*, 2023, **14**, 550–556.

43 E. Boutin, M. Wang, J. Lin, M. Mesnage, D. Mendoza, B. Lassalle-Kaiser, C. Hahn, T. Jaramillo and M. Robert, *Angew. Chem. Int. Ed.*, 2019, **58**, 16172–16176.

44 A. Varela, N. RanjbarSahraie, J. Steinberg, W. Ju, H. Oh and P. Strasser, *Angew. Chem. Int. Ed.*, 2015, **54**, 10758–10762.

45 W. Ju, A. Bagger, X. Wang, Y. Tsai, F. Luo, T. Möller, H. Wang, J. Rossmeisl, A. Varela and P. Strasser, *ACS Energy Lett.*, 2019, **4**, 1663–1671.

46 S. Nitopi, E. Bertheussen, S. Scott, X. Liu, A. Engstfeld, S. Horch, B. Seger, I. Stephens, K. Chan, C. Hahn, J. Nørskov, T. Jaramillo and I. Chorkendorff, *Chem. Rev.*, 2019, **119**, 7610–7672.

47 G. Mangione, J. Huang, R. Buonsanti and C. Corminboeuf, *J. Phys. Chem. Lett.*, 2019, **10**, 4259–4265.

48 S. Ikeda, T. Takagi and K. Ito, *Bull. Chem. Soc. Jpn.*, 1987, **60**, 2517–2522.

49 J. Fischer, T. Lehmann and E. Heitz, *J. Appl. Electrochem.*, 1981, **11**, 743–750.

50 M. Marx, H. Frauendorf, A. Spannenberg, H. Neumann and M. Beller, *JACS Au*, 2022, **2**, 731–744.

51 D. Esrafilzadeh, A. Zavabeti, R. Jalili, P. Atkin, J. Choi, B. J. Carey, R. Brkljac
a, A. P. O'Mullane, M. D. Dickey, D. L. Officer, D. R. MacFarlane, T. Daeneke and K. Kalantar-Zadeh, *Nat. Commun.*, 2019, **10**, 865.

52 J. P. Perdew, K. Burke and M. Ernzerhof, *Phys. Rev. Lett.*, 1996, **77**, 3865–3868.

53 S. Grimme, *J. Comput. Chem.*, 2006, **27**, 1787–1799.

54 S. Grimme, J. Antony, S. Ehrlich and H. Krieg, *J. Chem. Phys.*, 2010, **132**, 154104.

55 S. Grimme, S. Ehrlich and L. Goerigk, *J. Comput. Chem.*, 2011, **32**, 1456–1465.

56 G. Kresse and D. Joubert, *Phys. Rev. B*, 1999, **59**, 1758–1775.

57 S. L. Dudarev, A. I. Liechtenstein, M. R. Castell, G. A. D. Briggs and A. P. Sutton, *Phys. Rev. B*, 1997, **56**, 4900–4908.

58 S. L. Dudarev, G. A. Botton, S. Y. Savrasov, C. J. Humphreys and A. P. Sutton, *Phys. Rev. B*, 1998, **57**, 1505–1509.

59 J. Paier, C. Penschke and J. Sauer, *Chem. Rev.*, 2013, **113**, 3949–3985.

60 P. E. Blöchl, O. Jepsen and O. K. Andersen, *Phys. Rev. B*, 1994, **49**, 16223–16233.

61 K. Chan, C. Tsai, H. A. Hansen and J. K. Nørskov, *ChemCatChem*, 2014, **6**, 1899–1905.

62 J. K. Nørskov, J. Rossmeisl, A. Logadottir, L. Lindqvist, J. R. Kitchin, T. Bligaard and H. Jónsson, *J. Phys. Chem. B*, 2004, **108**, 17886–17892.

63 K. Mathew, V. S. C. Kolluru and R. G. Hennig, *VASPsol: Implicit solvation and electrolyte model for density-functional theory*, 2018, `https://github.com/henniggroup/VASPsol`.

64 K. Mathew, R. Sundararaman, K. Letchworth-Weaver, T. A. Arias and R. G. Hennig, *J. Chem. Phys.*, 2014, **140**, 084106.

65 K. Mathew, V. S. C. Kolluru, S. Mula, S. N. Steinmann and R. G. Hennig, *J. Chem. Phys.*, 2019, **151**, 234101.

66 G. Inc., *VASPsol convergence issue for CeO2(111)*, 2018, `https://github.com/henniggroup/VASPsol/issues/36`.

67 C. Dupont, O. Andreussi and N. Marzari, *J. Chem. Phys.*, 2013, **139**, 214110.

68 T. D. Kühne, M. Iannuzzi, M. D. Ben, V. V. Rybkin, P. Seewald, F. Stein, T. Laino, R. Z. Khaliullin, O. Schütt, F. Schiffmann, D. Golze, J. Wilhelm, S. Chulkov, M. H. Bani-Hashemian, V. Weber, U. Borštnik, M. Taillefumier, A. S. Jakobovits, A. Lazzaro, H. Pabst, T. Müller, R. Schade, M. Guidon, S. Andermatt, N. Holmberg, G. K. Schenter, A. Hehn, A. Bussy, F. Belleflamme, G. Tabacchi, A. Glöß, M. Lass, I. Bethune, C. J. Mundy, C. Plessl, M. Watkins, J. VandeVondele, M. Krack and J. Hutter, *J. Chem. Phys.*, 2020, **152**, 194103.

69 R. Sundararaman and W. A. Goddard, *J. Chem. Phys.*, 2015, **142**, 064107.

70 O. Andreussi, I. Dabo and N. Marzari, *J. Chem. Phys.*, 2012, **136**, 064102.

71 D. Gunceler, K. Letchworth-Weaver, R. Sundararaman, K. A. Schwarz and T. A. Arias, *Modell. Simul. Mater. Sci. Eng.*, 2013, **21**, 074005.

72 R. Sundararaman, K. Letchworth-Weaver, K. A. Schwarz, D. Gunceler, Y. Ozhabes and T. Arias, *SoftwareX*, 2017, **6**, 278–284.

73 M. Busch, R. Wang, A. Hellman, J. Rossmeisl and H. Grönbeck, *J. Phys. Chem. C*, 2018, **122**, 216–226.

74 S. Siahrostami, A. Verdaguer-Casadevall, M. Karamad, D. Deiana, P. Malacrida, B. Wickman, M. Escudero-

Escribano, E. Paoli, R. Frydendal, T. Hansen, I. Chorkendorff and J. Stephens, I. E. L. Rossmeisl, *Nat. Mater.*, 2013, **12**, 1137–1143.

75 W. Ju, A. Bagger, G. Hao, A. Varela, I. Sinev, V. Bon, B. Roldan Cuenya, S. Kaskel, J. Rossmeisl and P. Strasser, *Nature Commun.*, 2017, **8**, 944–.

76 F. Song, M. Busch, B. Lassalle-Kaiser, C. Hsu, E. Petkucheva, M. Bensimon, H. Chen, C. Corminboeuf and X. Hu, *ACS Cent. Sci.*, 2019, **5**, 558–568.

77 A. Groß, *Curr. Opin. Electrochem.*, 2021, **27**, 100684.

78 A. Groß, *J. Phys. Chem. C*, 2022, **126**, 11439–11446.

79 K. Alongi and G. Shields, *Annu. Rep. Comput. Chem.*, 2010, **6**, 113–138.

80 J. Ho, *Aust. J. Chem.*, 2014, **67**, 1441–1460.

81 M. Busch, E. Ahlberg, E. Ahlberg and K. Laasonen, *ACS Omega*, 2022, **7**, 17369–17383.

82 M. Busch, E. Ahlberg and K. Laasonen, *Phys. Chem. Chem. Phys.*, 2021, **23**, 11727–11737.

83 D. R. Lide, *CRC Handbook of Chemistry and Physic*, CRC Press Inc; 84th Edition, 2003.

84 M. e. Frisch, G. Trucks, H. Schlegel, G. Scuseria, M. Robb, J. Cheeseman, G. Scalmani, V. Barone, G. Petersson, H. Nakatsuji *et al.*, *Gaussian 16*, 2016.

85 Y. Zhao and D. G. Truhlar, *Theor. Chem. Acc.*, 2008, **120**, 215–241.

86 A. V. Marenich, C. J. Cramer and D. G. Truhlar, *J. Phys. Chem. B*, 2009, **113**, 6378—-6396.

87 U. J. Etim, C. Zhang and Z. Zhong, *Nanomaterials*, 2021, **11**, 3265.

88 H. Li, J. Zhao, L. Luo, J. Du and J. Zeng, *Acc. Chem. Res.*, 2021, **54**, 1454–1464.

89 A. F. Hollemannn and N. Wiberg, *Anorganische Chemie*, Walter de Gruyter, Berlin, 102nd edn., 2007.

90 M. Busch, E. Ahlberg and K. Laasonen, *Chem, Eur. J.*, 2022, **28**, e202201667.

91 D. Channei, S. Phanichphant, A. Nakaruk, S. Mofarah, P. Koshy and C. Sorrell, *Catalysts*, 2017, **7**, 45.

92 Y. Ma, Y. Ma, G. Giuli, H. Euchner, A. Groß, G. O. Lepore, F. d'Acapito, D. Geiger, J. Biskupek, U. Kaiser, H. M. Schütz, A. Carlsson, T. Diemant, R. J. Behm, M. Kuenzel, S. Passerini and D. Bresser, *Adv. Energy Mater.*, 2020, **10**, 2000783.

93 T. X. T. Sayle, S. C. Parker and D. C. Sayle, *Chem. Commun.*, 2004, 2438.

94 M. Fronzi, A. Soon, B. Delley, E. Traversa and C. Stampfl, *J. Chem. Phys.*, 2009, **131**, 104701.

95 N. V. Skorodumova, M. Baudin and K. Hermansson, *Phys. Rev. B*, 2004-02, **69**, 075401.

96 M. Nolan, S. C. Parker and G. W. Watson, *Surf. Sci.*, 2005, **595**, 223–232.

97 D. O. Scanlon, N. M. Galea, B. J. Morgan and G. W. Watson, *J. Phys. Chem. C*, 2009, **113**, 11095–11103.

98 Y.-L. Song, L.-L. Yin, J. Zhang, P. Hu, X.-Q. Gong and G. Lu, *Surf. Sci.*, 2013-12, **618**, 140–147.

99 R. Bruckner, *Reaktionsmechanismen*, Spektrum Akademischer Verlag, 2nd edn., 2002.

100 K. P. C. Vollhardt and N. E. Schore, *Organische Chemie*, Wiley-VCH Verlag, Weinheim, Germany, 5th edn., 2011.

101 R. F. Heck and J. P. Nolley, *J. Org. Chem.*, 1972, **37**, 2320–2322.

102 A. Wurtz, *Annalen der Chemie und Pharmacie*, 1855, **96**, 364–375.

103 K. Yoshikawa, M. Kaneeda and H. Nakamura, *Energy Procedia*, 2017, **114**, 2481–2487.

104 N. Baumann, J. Lan and M. Iannuzzi, *J. Chem. Phys.*, 2021, **154**, 094702.

105 M. Wang, M. Shen, X. Jin, J. Tian, Y. Zhou, Y. Shao, L. Zhang, Y. Li and J. Shi, *Nanoscale*, 2020, **12**, 12374–12382.

106 C. Elschenbroich and A. Salzer, *Organometallics*, Wiley-VCH Verlag, Weinheim, Germany, 2nd edn., 1992.

107 A. Visibile, R. B. Wang, A. Vertova, S. Rondinini, A. Minguzzi, E. Ahlberg and M. Busch, *Chem. Mater.*, 2019, **31**, 4787–4792.

108 S. Sakong, D. Mahlberg, T. Roman, M. Li, M. Pandey and A. Groß, *J. Phys. Chem. C*, 2020, **124**, 27604–27613.

109 M. Busch, N. B. Halck, U. I. Kramm, S. Siahrostami, P. Krtil and J. Rossmeisl, *Nano Energy*, 2016, **29**, 126–135.

110 M. I. Alvarado-Ávila, E. Toledo-Carrillo and J. Dutta, *ACS Omega*, 2022, **7**, 37465–37475.

111 C. McCrory, S. Jung, J. Peters and T. Jaramillo, *J. Am. Chem. Soc.*, 2013, **133**, 16977–16987.

112 C. McCrory, S. Jung, I. Ferrer, S. Chatman, J. Peters and T. Jaramillo, *J. Am. Chem. Soc.*, 2015, **137**, 4347–4367.

113 I. Roger and M. Symes, *ACS Appl. Mater. Interfaces*, 2017, **9**, 472–478.

114 R. Frydendal, M. Busch, N. Halck, E. Paoli, P. Krtil, I. Chorkendorff and J. Rossmeisl, *ChemCatChem*, 2015, **7**, 149–154.

115 Y. Gorlin, C. Chung, J. Benck, D. Nordlund, L. Seitz, T. Weng, D. Sokaras, B. Clemens and T. Jaramillo, *J. Am. Chem. Soc.*, 2014, **136**, 4920–4926.

116 G. Blyholder, *J. Phys. Chem.*, 1964, **68**, 2772–2777.

117 H. Staudinger, *Justus Liebigs Ann. Chem.*, 1907, **356**, 51–123.

118 H. H. Heenen, H. Shin, G. Kastlunger, S. Overa, J. A. Gauthier, F. Jiao and K. Chan, *Energy Environ. Sci.*, 2022, **15**, 3978–3990.

119 E. T. Seidl and H. F. I. I. I. Schaefer, *J. Am. Chem. Soc.*, 1991, **113**, 5195–5200.

120 R. Huisgen and P. Otto, *J. Am. Chem. Soc.*, 1968, **90**, 5342–5343.

121 H. Staudinger, *Ber. Dtsch. Chem. Ges.*, 1905, **38**, 1735–1739.

122 E. Wedekind, *Ber. Dtsch. Chem. Ges.*, 1901, **34**, 2070–2077.

123 E. Wedekind and W. Weisswange, *Ber. Dtsch. Chem. Ges.*, 1906, **39**, 1631–1646.

124 E. Wedekind, *Justus Liebigs Ann. Chem.*, 1902, **323**, 246–257.

125 G. B. Kistiakowsky and K. Sauer, *J. Am. Chem. Soc.*, 1958, **80**, 1066–1071.

126 K. Aida, M. Hirao, A. Funabashi, N. Sugimura, E. Ota and J. Yamaguchi, *Chem*, 2022, **8**, 1762–1774.

127 C. Huang, W. Ma, X. Zheng, M. Xu, X. Qi and Q. Lu, *J. Am. Chem. Soc.*, 2022, **144**, 1389–1395.

128 E. J. Kantorowski and M. J. Kurth, *Tetrahedron*, 2000, **56**, 4317–4353.

129 M. Polanyi and A. L. Szabo, *Trans. Faraday Soc.*, 1934, **30**, 508.

130 A. G. Davies and J. Kenyon, *Q. Rev. Chem. Soc.*, 1955, **9**, 203–228.